Nanoelectrochemistry

International Edition: DOI: 10.1002/anie.201802083
German Edition: DOI: 10.1002/ange.201802083

Dynamic Changes in the Structure, Chemical State and Catalytic Selectivity of Cu Nanocubes during CO_2 Electroreduction: Size and Support Effects

*Philipp Grosse[+], Dunfeng Gao[+], Fabian Scholten, Ilya Sinev, Hemma Mistry, and Beatriz Roldan Cuenya**

Abstract: *In situ and operando spectroscopic and microscopic methods were used to gain insight into the correlation between the structure, chemical state, and reactivity of size- and shape-controlled ligand-free Cu nanocubes during CO_2 electroreduction (CO_2RR). Dynamic changes in the morphology and composition of Cu cubes supported on carbon were monitored under potential control through electrochemical atomic force microscopy, X-ray absorption fine-structure spectroscopy and X-ray photoelectron spectroscopy. Under reaction conditions, the roughening of the nanocube surface, disappearance of the (100) facets, formation of pores, loss of Cu and reduction of CuO_x species observed were found to lead to a suppression of the selectivity for multi-carbon products (i.e. C_2H_4 and ethanol) versus CH_4. A comparison with Cu cubes supported on Cu foils revealed an enhanced morphological stability and persistence of Cu^I species under CO_2RR in the former samples. Both factors are held responsible for the higher C_2/C_1 product ratio observed for the Cu cubes/Cu as compared to Cu cubes/C. Our findings highlight the importance of the structure of the active nanocatalyst but also its interaction with the underlying substrate in CO_2RR selectivity.*

In recent years interest in understanding the parameters that govern the electrochemical reduction of CO_2 (CO_2RR) has increased. The knowledge is used to design catalysts with high selectivity for valuable chemicals and fuels.[1] Among these parameters, the catalyst structure and chemical state are of particular importance.[2–4] Compared to polycrystalline Cu electrodes, nanostructured Cu catalysts have shown a significantly improved CO_2RR performance, attributed to grain boundaries,[5,6] Cu(100) facets,[7–12] increased roughness,[13] defects,[14–16] low-coordinated sites,[17–19] and the presence of subsurface oxygen and Cu^I species.[20–29]

Previous studies[9–11] on Cu single crystals have shown the improved C–C coupling performance of (100) facets, which was further confirmed by the high selectivity towards ethylene observed on cube-shaped Cu catalysts.[7,8,16,21,30–36] However, the presence of (100) facets is not the only factor responsible for the superior activity and selectivity of cube-shaped Cu catalysts, with surface roughness, subsurface oxygen and Cu^I species or Cu/Cu^I interfaces formed and/or stabilized under reaction conditions also playing a very important role.[21] The function of oxygen in such structures is particularly intriguing, since on Cu(100) surfaces it was discussed to contribute to the formation of oxygenated hydrocarbons.[37] The complexity arising from the multiple factors affecting the catalytic performance of cube-shaped Cu catalysts requires a systematic study of the evolution of their structure and oxidation state under operando CO_2RR conditions.

This work focuses on the understanding of the relative importance of the different factors responsible for specific selectivity trends observed for Cu catalysts during CO_2RR, namely, the presence and stability of Cu(100) facets, defect sites, and the content of Cu^I species and/or subsurface oxygen. By electrochemically growing ligand-free Cu cubes on C supports and comparing with analogous samples supported on Cu foils, we were able to reveal the intrinsic behavior of the cube-shaped Cu NPs catalysts and their dynamic evolution under CO_2RR conditions.

Size-dependent changes in the morphology and composition of Cu cube samples electrodeposited on carbon paper were investigated ex situ through scanning electron microscopy (SEM) and energy dispersive X-ray spectroscopy (EDX) before and after CO_2RR (Figure 1 and Figures S1 and S2 in the Supporting Information). In all samples the Cu cubes were found to decrease in size in the course of the first hour of the reaction. Furthermore, in this process the originally flat facets and sharp edges of the Cu cubes were found to roughen, resulting in a porous nanocube surface (see Figure 1).

Operando electrochemical atomic force microscopy (EC-AFM) measurements carried out on a sample with approximately 100 nm large cubes also revealed significant changes in their morphology already prior to the actual CO_2RR (Figure 2). Sample immersion in the aqueous 0.1M $KHCO_3$ electrolyte at open circuit potential was observed to lead to the formation of "cracks" on the cube facets. These cracks are

[*] P. Grosse,[+] D. Gao,[+] F. Scholten, I. Sinev, H. Mistry, B. Roldan Cuenya
Department of Physics, Ruhr-University Bochum
44780 Bochum (Germany)
H. Mistry, B. Roldan Cuenya
Department of Physics, University of Central Florida
Orlando, FL 32816 (USA)
B. Roldan Cuenya
Department of Interface Science
Fritz-Haber Institute of the Max Planck Society
14195 Berlin (Germany)
E-mail: Roldan@fhi-berlin.mpg.de
[+] These authors contributed equally to this work.
Supporting information and the ORCID identification number(s) for the author(s) of this article can be found under: https://doi.org/10.1002/anie.201802083.

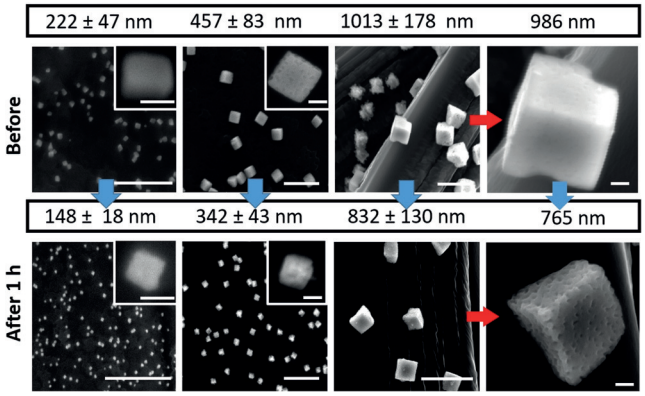

Figure 1. SEM images from size-controlled Cu cube samples electrodeposited on carbon paper acquired before and after CO_2RR at −1.05 V for 1 h. The scale bars in the main panels are 2 µm, those in the insets and in the images of the last column are 200 nm.

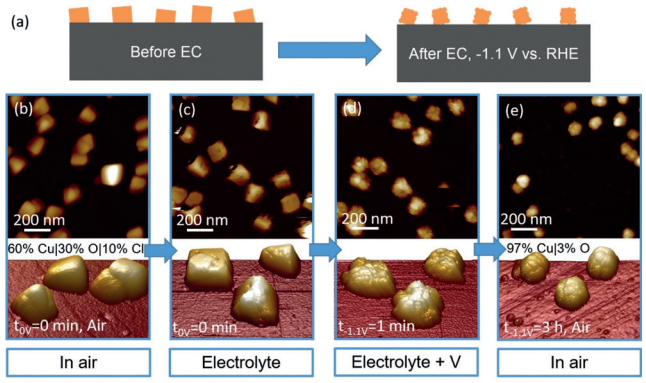

Figure 2. a) Schematic representation of the morphological evolution of Cu cube catalysts. b–e) AFM images of Cu cubes electrodeposited on highly oriented pyrolytic graphite (HOPG) acquired in air (b), and operando EC-AFM measurements in a CO_2-saturated 0.1 M $KHCO_3$ aqueous solution at open circuit potential (c), at −1.1 V versus RHE in the same electrolyte for 1 minute (d), and after 3 h under the same conditions as in (d) and subsequent air exposure (e).

likely the result of mechanical stress taking place during the solvation of Cl^- ions while being transferred from the cubes to the electrolyte. SEM-EDX data revealed that Cl was present throughout the entire Cu volume in the as prepared samples and therefore, the loss of Cl leads to drastic structural changes in the entire cube volume.

A 1 minute potential pulse at −1.1 V versus reversible hydrogen electrode (RHE) resulted in the further roughening of the nanocube surface, loss of sharp corners and edges, and a decrease in the edge length of approximately 10%. The latter is assigned to the initial reduction of Cu_2O to Cu as well as some loss of Cu. After 3 h CO_2RR at −1.1 V versus RHE, an additional 10% decrease of the NP size was observed, with rough spherical-like NP shapes.

X-ray-induced Cu LMM Auger electron spectra (XAES) were acquired from pristine C-supported Cu cubes (220 nm) before and after CO_2RR for 1 h at −1.1 V versus RHE in an ultrahigh vacuum (UHV) XPS system directly interfaced to an electrochemical cell. Thus, the sample could be transferred in vacuum to avoid re-oxidation.[21] Additional Cu 2p XPS data are also included in Figure S3. A surface composition of the pristine C-supported Cu cubes of 52% Cu_2O, 22% $CuCl_2$, 23% CuCl, and 3% metallic Cu was obtained before reaction, Figure 3. After the electrochemical treatment, the cubes are

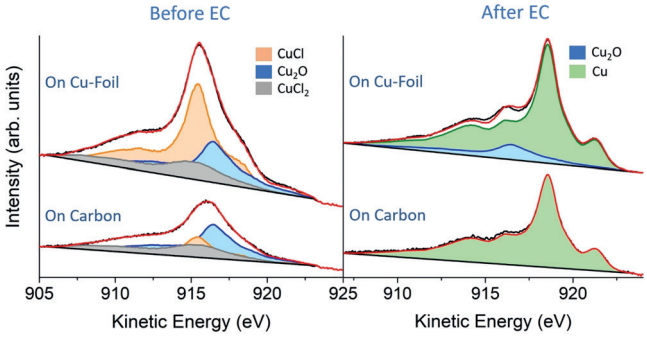

Figure 3. Quasi in situ Cu Auger LMM XAES spectra of 220 nm Cu cubes electrodeposited on C paper and 250 nm cubes deposited on a Cu foil acquired before (left) and after 1 hour of CO_2RR at −1.1 V versus RHE (right).

mostly reduced, with only 4.6% Cu_2O detected. Interestingly, a higher content of Cu^I species (13%) was detected after CO_2RR on similarly synthesized Cu cubes supported on a Cu foil, and no Cu^I at all in the pristine Cu foil support after CO_2RR (Figure S4). The latter finding highlights the key role of having a Cu cube/Cu foil interaction for the stabilization of Cu^I species.

To gain further insight into the stability of Cl, Cu^I species, and subsurface oxygen in our Cu cubes under CO_2RR, operando X-ray absorption fine-structure (XAFS) measurements were conducted on 120 nm Cu cubes, Figures 4 and 5 (see also Figures S5, S6, and S7 in the SI for more details). As compared to XPS and XAES, probing about 10 nm below the surface, XAFS is a bulk sensitive technique that reveals the overall change in the structure and composition of the

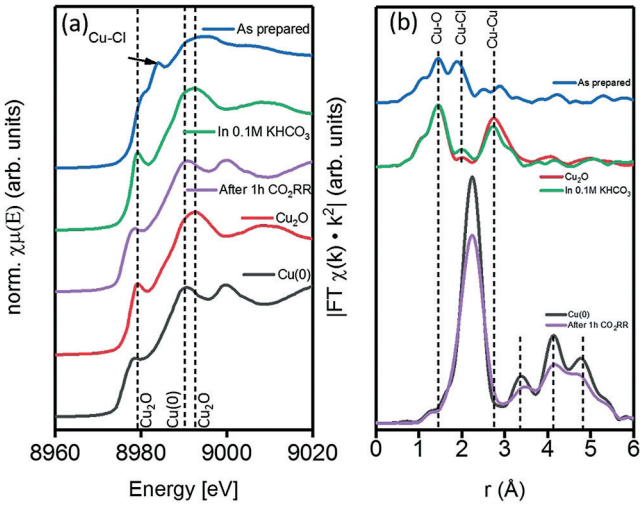

Figure 4. Normalized XANES region (a) and Fourier-transform magnitudes of k^2-weighted EXAFS data of pristine Cu cubes (b) measured as prepared, in 0.1 M $KHCO_3$ at open circuit potential and in the same electrolyte after 1 h of CO_2RR at −1.1 V versus RHE.

Cu cubes. The as prepared state of the Cu cubes shows a mixture of Cu_2O and $CuCl_x$, which almost immediately changes fully into Cu_2O upon becoming in contact with the electrolyte.

In CO_2-saturated 0.1M $KHCO_3$, the spectrum resembles greatly the Cu_2O reference, with only a very small difference where the Cl-feature was previously observed and a small decrease of the Cu–O feature. After 1 h at −1.1 V versus RHE, the spectrum obtained for the Cu cubes resembles that of metallic Cu. The Fourier Transform (FT) data obtained for the Cu cubes in the electrolyte after 1 h CO_2RR at −1.1 V versus RHE are less intense in comparison to a bulk Cu foil, indicating a lower atomic coordination and/or enhanced disorder. From the first shell Cu–Cu fit after 1 h of applied potential, a coordination number (CN) of 10.8 was obtained for the Cu cubes (vs. 12 expected for bulk fcc-Cu). The lower CN values might be indicative of the formation and growth of pores on the Cu cubes under reaction conditions or the partial disruption of the nanocubes, leading to an increased surface roughness. The operando EC-AFM data also revealed the formation of cracks (defects) on the Cu cubes even before applying the potential once they were exposed to the electrolyte. The porous structure seen by SEM can also be a result of the progressive CuO_x reduction during the reaction. Under reaction conditions, these pores as well as the cube corners and edges appear more prone to dissolution than the higher coordinated flat facets.

Since Cu^I species[37] have been suggested to play an important role in CO_2RR selectivity, in order to better detect small amounts of Cu–O species an additional analysis of the XAFS data by wavelet-transform[38] (WT) was applied (Figure 5). Details on this analysis are given in the Suppl. documents. After processing the measured spectra and doing the Morlet WT, the spectra were normalized to the highest signal, allowing subtraction of measured reference materials. The Cu cubes on C in their as prepared state display a large feature at $R \approx 1.4$ Å and $k \approx 3.9$ Å^{-1} which represents the Cu–O shell, whereas at a slightly higher distance ($R \approx 2$ Å, $k \approx 7$ Å^{-1}) the interaction of Cu with the heavier Cl atoms is visible. For the as prepared sample, only a faint Cu–Cu 1st and 2nd neighbor interaction is observed after the subtraction of a Cu_2O reference from the pristine Cu cubes, indicating that the sample consists almost exclusively of Cu_2O and $CuCl_x$. In the electrolyte, the $CuCl_x$ feature immediately disappears and a Cu–O–Cu feature arises at $R \approx 3$ Å and $k \approx 4$ Å^{-1}. In addition, the magnitude of the Cu–O component decreases slightly. After 1 hour of CO_2RR, the most prominent feature is that of the Cu–Cu first shell ($R \approx 2.3$ Å, $k \approx 7$ Å^{-1}). The pristine Cu cubes resemble almost exactly the metallic Cu reference after 1 h of CO_2RR. A deconvolution of the Cu XANES region of pristine Cu cubes in 0.1M $KHCO_3$ with Cu, Cu_2O, and CuO standards, Figure S7, yields a composition of 99% Cu and 1% (within the error margin) Cu_2O after 1 h of CO_2RR. CuO could not be reasonable fitted. These findings are in good accordance with the XPS surface analysis indicating that for the Cu cube/C system, no Cu_2O species remain after 1 h of reaction either at the surface (XPS) or in sub-surface regions (XAFS), which is in clear contrast with previous findings for Cu cubes/Cu foil (Figure 3).[21,22]

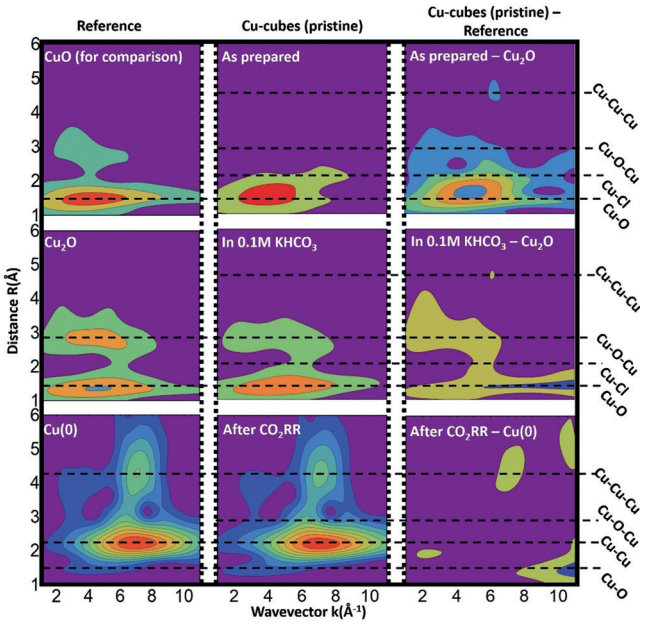

Figure 5. Wavelet transform of Cu cubes as prepared, in 0.1 M $KHCO_3$, and after 1 h of CO_2RR as well as the bulk references used. The height is normalized to 1 and the subtracted images scaled by a factor of two for better visibility.

After observing drastic changes in the morphology and chemical composition of the samples under operando reaction conditions within the first 1–3 hours, the electrochemical performance was studied in order to gain insight into structure/chemical-state/reactivity correlations. The background signal from the C-paper support was subtracted from all data presented as shown in Figure S8. A comparison between HER Faradaic efficiency (parasitic reaction) and the sum of the Faradaic efficiency of all products from CO_2RR is displayed in Figure 6. Detailed information on the different products detected can be found in Figure 7 for the 220 nm Cu cubes and in Figures S9, S10 and S11. Similar trends for small Cu–Au cubic NPs were reported in ref. [39].

For the stability tests, Cu cubes of three different initial sizes were investigated at −1.05 V versus RHE, Figure 6. This potential was chosen since we expect to see the highest selectivity towards C_2–C_3 products.[40] The total CO_2RR FE was found to increase with increasing Cu cube size, and achieves an initial value of approximately 75% on the 580 nm cubes. This is assigned to the enhanced morphological stability of the larger cubes. A second general trend, independent of size, is a decrease in Faradaic efficiency for CO_2RR and increase in HER over time. An exception is the sample containing 220 nm Cu cubes, which starts already with higher Faradaic efficiency for HER over CO_2RR. The smaller cube size on the weakly binding C support leads to a lower stability of the Cu cubes, leading to the loss of material into the electrolyte and possible subsequent re-deposition as small clusters on the support and Cu cubes. Such low-coordinated structures were found to result in an increase in the H_2 and CO production and decrease in the formation of hydrocarbons, that is, they favor HER over CO_2RR.[41,42] This

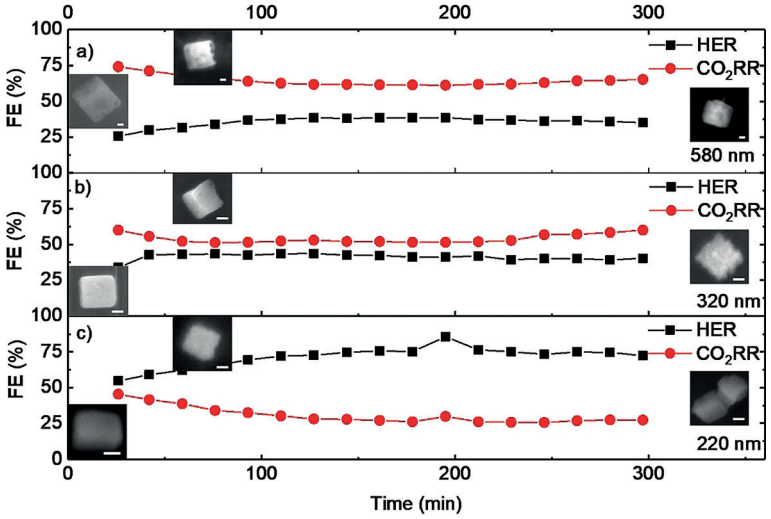

Figure 6. Faradaic efficiency for CO_2RR and HER at -1.05 V versus RHE recorded during 5 h for samples with different Cu cube sizes (580 nm, 320 nm and 220 nm). The insets display SEM images of typical Cu cubes measured after different reaction times. The size of the scale bars is: 100 nm.

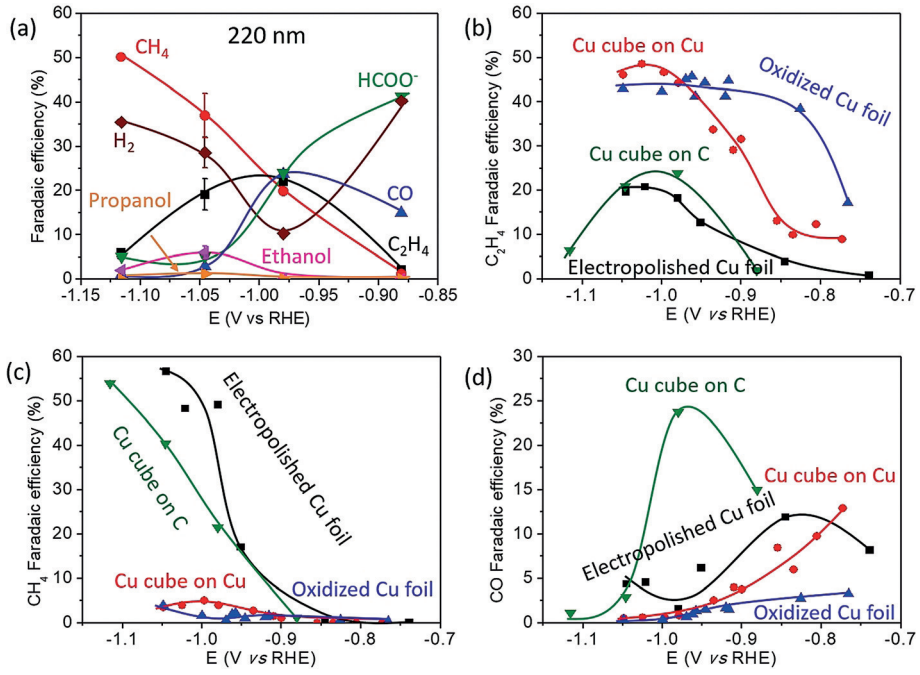

Figure 7. a) Faradaic efficiency of pristine 220 nm Cu cubes on C as a function of applied potential obtained after 1 h of CO_2RR. Faradaic efficiencies for C_2H_4 (b), CH_4 (c), and CO (d) are also shown for the pristine 220 nm Cu cubes on C, 250 nm Cu cubes on Cu foil and two reference Cu foils electropolished and O_2-plasma treated (20 W, 2 minutes, 400 mTorr[21,22]).

correlates with the observed morphological changes shown in Figures 1 and 2, where a rounding of corners and edges and roughening of the facets is observed.

Figure 7a displays the FE data for the pristine 220 nm Cu cubes on C measured as a function of the applied potential after 1 h of CO_2RR. The production of C_2 and C_3 products peaks around −1.0 V versus RHE, whilst hydrogen evolution is the lowest at this potential. At potentials more negative than −1.0 V versus RHE, C_2/C_3 products decline, whilst methane production keeps increasing.

The FE for C_2H_4, CH_4 and CO as a function of the applied potential for the pristine 220 nm Cu cubes on C together with similarly synthesized 250 nm Cu cubes supported on a Cu foil as well as electropolished and O_2-plasma-treated Cu foils are shown in Figure 7(b–d). A very strong support-effect is evident, with the Cu cubes grown in the weakly-interacting C support displaying a higher overpotential and much lower FE for C_2–C_3 products than the similarly-sized Cu cubes on the Cu foil. In fact, as can be seen in Figure 7(c), the production of CH_4 of the Cu cubes on C resembles the metallic electropolished Cu foil, although the CO production of the Cu cubes on C is much higher, Figure 7(d). It is remarkable that the pristine Cu cubes on the Cu foil, which were found to better stabilize Cu^I species under reaction conditions (Figure 3), behave similarly to the O_2-plasma treated Cu foils. Therefore, we can confirm a direct correlation between the stabilization of Cu^I/Cu interfaces (Cu cubes on Cu foil) and the selectivity for C_2–C_3 products, since metallic Cu cubes supported on C are more selective for C_1 products. This is however not the only reason for the change in the selectivity. Even more important are the drastic structural changes observed for the Cu cubes on C. The roughening of the Cu(100) facets, partial loss of the cubic shape and formation of pores as well as detachment from the surface play a critical role in the selectivity switch reported here.

A simple electrochemical method for the synthesis of cube-shaped nanoparticles of tunable size supported on carbon substrates is presented here. Dynamic morphological and chemical transformations of Cu cubes during CO_2RR were monitored using operando EC-AFM and XAFS. Drastic changes in the cube morphology were found to take place for the Cu cubes on C under CO_2RR conditions, including the roughening and loss of (100) facets, loss of Cu atoms from edge and corner sites, and the reduction of CuO_x species.

The selectivity for CO_2RR versus HER was found to decrease with decreasing cube size, which was assigned to more drastic changes in the cube morphology taking place under CO_2RR conditions over smaller cubes. In contrast with the findings previously reported for Cu cubes grown on Cu foils, a surprisingly high selectivity for CH_4 as compared to

C_2H_4 was observed when deposited on C. The observed morphological instability of the Cu cubes on C versus those deposited on Cu, together with the absence of stable Cu^I species in the former samples are considered responsible for the preferred selectivity for C_1 products.

Experimental Section

A mixture of 5 mM copper sulfate-pentahydrate ($CuSO_4 \cdot 5H_2O$) and 5 mM potassium chloride (KCl) was used as starting material. Electrochemical cycling between an oxidizing (+0.55 V vs. RHE) and a reducing potential (+0.22 V vs. RHE) with varying number of cycles (1–100), depending on the desired cube size and coverage, lead to the electrodeposition of size- and shape-controlled Cu cubes with a narrow size distribution. Initially, a potential of −0.2 V versus Ag/AgCl was held for 8 s with a subsequent ramp to +0.4 V versus Ag/AgCl for 4 s at a ramp rate of 700 $mV s^{-1}$. Returning to the initial potential completes the cyclic voltammetry. Cu cube sizes ranging from 80 nm to 1.2 μm were obtained depending on the 1 mM–100 mM KCl and $CuSO_4 \cdot 5H_2O$ concentration, number of cycles, and applied potential. High surface area carbon paper was used as substrate (Toray Carbon Paper TGP-H-060). The Cu cubes on Cu foil were prepared as described in ref. [21].

Acknowledgements

This work was funded by the Cluster of Excellence RESOLV at RUB (EXC 1069) supported by the Deutsche Forschungsgemeinschaft and the German Federal Ministry of Education and Research (Bundesministerium für Bildung und Forschung BMBF) under grant number 03SF0523C-"CO2EKAT" and by the European Research Council (ERC-725915, OPERANDOCAT). Partial financial support from the U.S. National Science Foundation (NSF-Chemistry 1213182) is also greatly appreciated. The XAFS experiments were performed on beamline BM25A at the European Synchrotron Radiation Facility (ESRF), Grenoble, France. We are grateful to Aida Serrano Rubio and Germán Castro at the ESRF for providing assistance in using beamline BM25A.

Conflict of interest

The authors declare no conflict of interest.

Keywords: copper cubes · electroreduction · density functional calculations · nanoelectrochemistry · surface chemistry

How to cite: *Angew. Chem. Int. Ed.* **2018**, *57*, 6192–6197
Angew. Chem. **2018**, *130*, 6300–6305

[1] Y. Hori, A. Murata, R. Takahashi, S. Suzuki, *J. Chem. Soc. Chem. Commun.* **1988**, 0, 17-19.
[2] H. Mistry, A. S. Varela, S. Kühl, P. Strasser, B. R. Cuenya, *Nat. Rev. Mater.* **2016**, *1*, 16009.
[3] R. Kortlever, J. Shen, K. J. P. Schouten, F. Calle-Vallejo, M. T. M. Koper, *J. Phys. Chem. Lett.* **2015**, *6*, 4073–4082.
[4] G. O. Larrazábal, A. J. Martín, J. Pérez-Ramírez, *J. Phys. Chem. Lett.* **2017**, *8*, 3933–3944.
[5] C. W. Li, M. W. Kanan, *J. Am. Chem. Soc.* **2012**, *134*, 7231–7234.
[6] A. M. Appel, *Nature* **2014**, *508*, 460–461.
[7] F. S. Roberts, K. P. Kuhl, A. Nilsson, *Angew. Chem. Int. Ed.* **2015**, *54*, 5179–5182; *Angew. Chem.* **2015**, *127*, 5268–5271.
[8] A. Loiudice, P. Lobaccaro, E. A. Kamali, T. Thao, B. H. Huang, J. W. Ager, R. Buonsanti, *Angew. Chem. Int. Ed.* **2016**, *55*, 5789–5792; *Angew. Chem.* **2016**, *128*, 5883–5886.
[9] K. J. P. Schouten, E. Pérez Gallent, M. T. M. Koper, *ACS Catal.* **2013**, *3*, 1292–1295.
[10] F. Calle-Vallejo, M. T. M. Koper, *Angew. Chem.* **2013**, *125*, 7423–7426.
[11] J. H. Montoya, C. Shi, K. Chan, J. K. Nørskov, *J. Phys. Chem. Lett.* **2015**, *6*, 2032–2037.
[12] D. Kim, C. S. Kley, Y. Li, P. Yang, *Proc. Natl. Acad. Sci. USA* **2017**, *114*, 10560–10565.
[13] R. Kas, R. Kortlever, H. Yilmaz, M. T. M. Koper, G. Mul, *ChemElectroChem* **2015**, *2*, 354–358.
[14] W. Tang, A. A. Peterson, A. S. Varela, Z. P. Jovanov, L. Bech, W. J. Durand, S. Dahl, J. K. Nørskov, I. Chorkendorff, *Phys. Chem. Chem. Phys.* **2012**, *14*, 76–81.
[15] R. B. Sandberg, J. H. Montoya, K. Chan, J. K. Nørskov, *Surf. Sci.* **2016**, *654*, 56–62.
[16] I. Zegkinoglou, A. Zendegani, I. Sinev, S. Kunze, H. Mistry, H. S. Jeon, J. Zhao, M. Y. Hu, E. E. Alp, S. Piontek, et al., *J. Am. Chem. Soc.* **2017**, *139*, 14360–14363.
[17] R. Reske, H. Mistry, F. Behafarid, B. Roldan Cuenya, P. Strasser, *J. Am. Chem. Soc.* **2014**, *136*, 6978–6986.
[18] H. Mistry, F. Behafarid, R. Reske, A. S. Varela, P. Strasser, B. Roldan Cuenya, *ACS Catal.* **2016**, *6*, 1075–1080.
[19] H. Mistry, R. Reske, P. Strasser, B. Roldan Cuenya, *Catal. Today* **2017**, *288*, 30–36.
[20] H. Mistry, A. S. Varela, C. S. Bonifacio, I. Zegkinoglou, I. Sinev, Y. W. Choi, K. Kisslinger, E. A. Stach, J. C. Yang, P. Strasser, et al., *Nat. Commun.* **2016**, *7*, 12123.
[21] D. Gao, I. Zegkinoglou, N. J. Divins, F. Scholten, I. Sinev, P. Grosse, B. Roldan Cuenya, *ACS Nano* **2017**, *11*, 4825–4831.
[22] D. Gao, F. Scholten, B. Roldan Cuenya, *ACS Catal.* **2017**, *7*, 5112–5120.
[23] C. Reller, R. Krause, E. Volkova, B. Schmid, S. Neubauer, A. Rucki, M. Schuster, G. Schmid, *Adv. Energy Mater.* **2017**, *7*, 1602114.
[24] A. Eilert, F. Cavalca, F. S. Roberts, J. Osterwalder, C. Liu, M. Favaro, E. J. Crumlin, H. Ogasawara, D. Friebel, L. G. M. Pettersson, et al., *J. Phys. Chem. Lett.* **2017**, *8*, 285–290.
[25] S. Lee, D. Kim, J. Lee, *Angew. Chem. Int. Ed.* **2015**, *54*, 14701–14705; *Angew. Chem.* **2015**, *127*, 14914–14918.
[26] D. Ren, Y. Deng, A. D. Handoko, C. S. Chen, S. Malkhandi, B. S. Yeo, *ACS Catal.* **2015**, *5*, 2814–2821.
[27] H. Xiao, W. A. Goddard, T. Cheng, Y. Liu, *Proc. Natl. Acad. Sci. USA* **2017**, *114*, 6685–6688.
[28] M. Favaro, H. Xiao, T. Cheng, W. A. Goddard, J. Yano, E. J. Crumlin, *Proc. Natl. Acad. Sci. USA* **2017**, *114*, 6706–6711.
[29] X. Wang, A. S. Varela, A. Bergmann, S. Kühl, P. Strasser, *ChemSusChem* **2017**, *10*, 4642–4649.
[30] Z. W. Ulissi, M. T. Tang, J. Xiao, X. Liu, D. A. Torelli, M. Karamad, K. Cummins, C. Hahn, N. S. Lewis, T. F. Jaramillo, et al., *ACS Catal.* **2017**, *7*, 6600–6608.
[31] X. Liu, J. Xiao, H. Peng, X. Hong, K. Chan, J. K. Nørskov, *Nat. Commun.* **2017**, *8*, 15438.
[32] Z. W. She, J. Kibsgaard, C. F. Dickens, I. Chorkendorff, J. K. Nørskov, T. F. Jaramillo, *Science* **2017**, *355*, eaad4998.
[33] W. Ju, A. Bagger, G. P. Hao, A. S. Varela, I. Sinev, V. Bon, B. Roldan Cuenya, S. Kaskel, J. Rossmeisl, P. Strasser, *Nat. Commun.* **2017**, *8*, 944.
[34] P. De Luna, R. Quintero-Bermudez, C.-T. Dinh, M. B. Ross, O. S. Bushuyev, P. Todorović, T. Regier, S. O. Kelley, P. Yang, E. H. Sargent, *Nat. Catal.* **2018**, *1*, 103–110.

[35] K. Jiang, R. B. Sandberg, A. J. Akey, X. Liu, D. C. Bell, J. K. Nørskov, K. Chan, H. Wang, *Nat. Catal.* **2018**, *1*, 111 – 119.
[36] B. Eren, R. S. Weatherup, N. Liakakos, G. A. Somorjai, M. Salmeron, *J. Am. Chem. Soc.* **2016**, *138*, 8207 – 8211.
[37] C. S. Le Duff, M. J. Lawrence, P. Rodriguez, *Angew. Chem. Int. Ed.* **2017**, *56*, 12919 – 12924; *Angew. Chem.* **2017**, *129*, 13099 – 13104.
[38] J. Timoshenko, A. Kuzmin, *Comput. Phys. Commun.* **2009**, *180*, 920 – 925.
[39] J. Monzó, Y. Malewski, R. Kortlever, F. J. Vidal-Iglesias, J. Solla-Gullón, M. T. M. Koper, P. Rodriguez, *J. Mater. Chem. A* **2015**, *3*, 23690 – 23698.
[40] Y. Hori, A. Murata, R. Takahashi, *J. Chem. Soc. Faraday Trans. 1* **1989**, *85*, 2309.
[41] H. Mistry, R. Reske, Z. Zeng, Z.-J. Zhao, J. Greeley, P. Strasser, B. Roldan Cuenya, *J. Am. Chem. Soc.* **2014**, *136*, 16473 – 16476.
[42] F. Behafarid, J. Matos, S. Hong, L. Zhang, T. S. Rahman, B. Roldan Cuenya, *ACS Nano* **2014**, *8*, 6671 – 6681.

Manuscript received: February 15, 2018
Accepted manuscript online: March 26, 2018
Version of record online: April 26, 2018

